

Visualizing Topography by Openness: A New Application of Image Processing to Digital Elevation Models

Ryuzo Yokoyama, Michio Shirasawa, and Richard J. Pike

Abstract

A new parameter, here termed *openness*, expressing the degree of dominance or enclosure of a location on an irregular surface, is developed to visualize topographic character. Openness is an angular measure of the relation between surface relief and horizontal distance. For angles less than 90° , it is equivalent to the internal angle of a cone, its apex at a DEM location, constrained by neighboring elevations within a specified radial distance. Openness incorporates the terrain line-of-sight, or viewshed, concept and is calculated from multiple zenith and nadir angles—here along eight azimuths. Openness has two viewer perspectives. Positive values, expressing openness above the surface, are high for convex forms, whereas negative values describe this attribute below the surface and are high for concave forms. Openness values are mapped by gray-scale tones. The emphasis of terrain convexity and concavity in openness maps facilitates the interpretation of landforms on the Earth's surface and its seafloor, and on the planets, as well as features on any irregular surface—such as those generated by industrial procedures.

Introduction

Relief maps and the parametric characterization of topography are essential to the interpretation of the land surface. Hill-shaded maps initially were drafted by landscape artists, but map precision and reproducibility were limited by the manual technique and its requisite cartographic skill (Raisz, 1931; Imhof, 1965; Alpha and Winter, 1971). The advent of the electronic computer and the digital elevation model (DEM) overcame these restrictions, and machine-made shaded-relief maps now are widely used to display topography (Yoeli, 1967; Horn and Brooks, 1989; Thelin and Pike, 1991; Vigil *et al.*, 2000). The technique is not without drawbacks of its own. Because a directional light source is required, for example, ridges and valleys intersecting that source are shown clearly while features parallel to the source can be difficult to identify. Attempts to mitigate this problem by multiple light sources have been only partially successful (Mark, 1992; Moore and Mark, 1992; Riehle *et al.*, 1997).

Other types of neighborhood operations centered on DEM grid points yield digital maps that display or extract topographic features (Tobler, 1969; Peucker and Douglas, 1975;

Weibel and Heller, 1991; Blaszczyński 1997; Guth, 2001). Terrain slope, curvature in both the XY and Z domains, relative relief, and slope azimuth are among the measures most commonly mapped from DEMs (Evans, 1972; Pike, 1988). Algorithms that implement the much-used DEM-to-watershed transformation, now an essential tool for hydrologic and geomorphic modeling, incorporate several such measures (Jenson and Domingue, 1988; ESRI, 1992). Like automated relief shading, however, all of these parameters are sensitive to the vagaries inherent in gridded height data (Carter, 1992). In particular, slope maps computed from DEMs commonly have an unsatisfactory wormlike appearance that reflects the method of contour gridding and obscures the true configuration of the land surface.

In this paper, we introduce a new concept of surface representation, provisionally termed *openness* for want of a better name. It is a novel method for digital terrain modeling—actually an image-processing technique—by which values of surface openness are calculated from a DEM, displayed in map form, and used to visualize landscapes. The resulting maps of openness superficially resemble digital images of shaded relief or slope angle, but emphasize dominant surface concavities and convexities. Values of openness require no light source, thus removing one limitation of relief shading, and are less affected by the DEM noise that afflicts most other parameters. After describing the technique, we present several maps of surface openness and discuss how they may be applied to the analysis and interpretation of topography.

Zenith and Nadir Angles

Before defining topographic openness, we must establish some angular relations between the point locations along individual DEM-derived profiles, and do this for viewer perspectives both above and below the surface. The first quantity to be extracted from these relations is elevation angle θ .

Figure 1 shows a sample of terrain heights in a DEM arrayed north-south and east-west at a constant spacing M , projected in Universal Transverse Mercator (UTM) coordinates, and centered on a point of interest (double circle). Each point in the DEM is described by (i, j, H) where i and j are column and row numbers and H is elevation. Figure 2 defines the geometric relation in profile between any two points $A(i_A, j_A, H_A)$ and $B(i_B, j_B, H_B)$ in the DEM, here showing a case where $H_A < H_B$. Horizontal distance P between A and B is given by

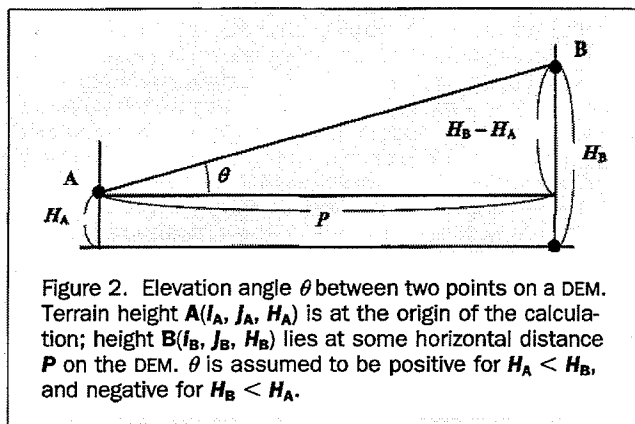
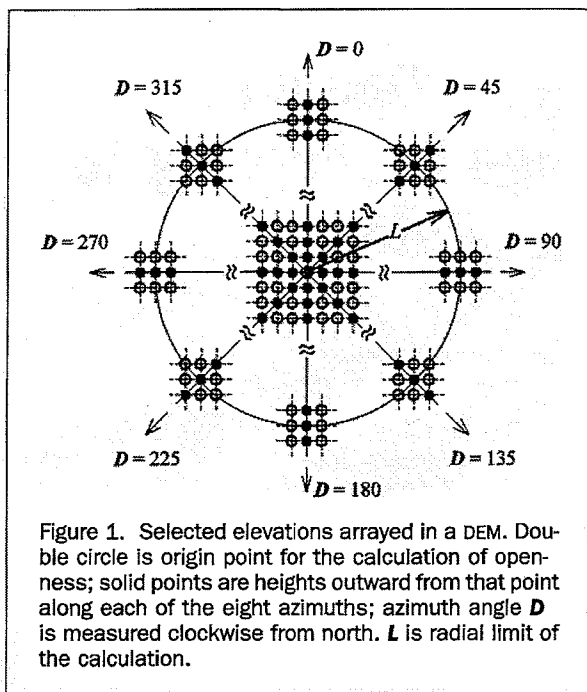
R. Yokoyama and M. Shirasawa are with the Department of Computer and Information Science, Faculty of Engineering, Iwate University, 4-3-5, Ueda, Morioka, Iwate, 020-8551 Japan (yokoyama@cis.iwate-u.ac.jp).

R.J. Pike is with the U.S. Geological Survey, M/S 975, 345 Middlefield Road, Menlo Park, CA 94025.

Photogrammetric Engineering & Remote Sensing
Vol. 68, No. 3, March 2002, pp. 257–265.

0099-1112/02/6803-257\$3.00/0

© 2002 American Society for Photogrammetry
and Remote Sensing



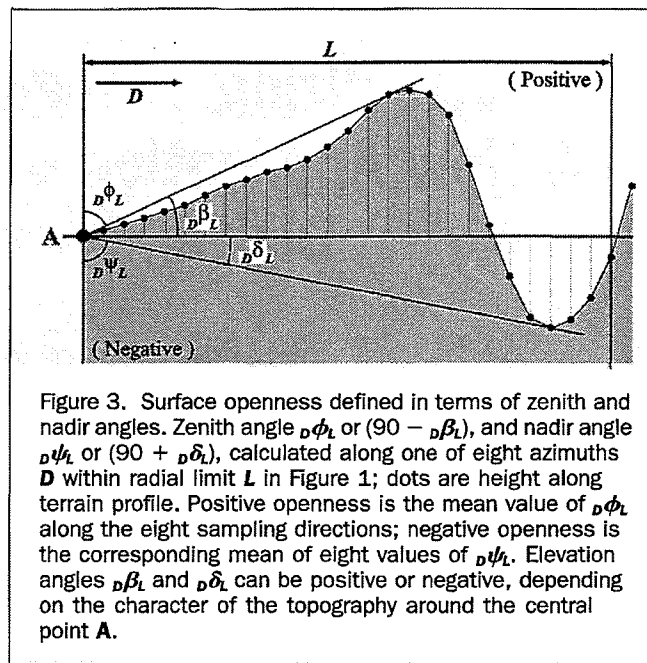
$$P = M \sqrt{(j_A - i_B)^2 + (j_A - j_B)^2} \quad (1)$$

and the elevation angle θ of line AB is

$$\theta = \tan^{-1} \left\{ \frac{(H_B - H_A)}{P} \right\}. \quad (2)$$

Angle θ is positive when $H_A < H_B$ and negative when $H_B < H_A$. A general treatment of P and θ would incorporate Earth's curvature, but this can be neglected because the calculation requires only small patches of terrain and thus short horizontal distances. Angle θ enables us to identify a $D-L$ set.

Definition 1: A $D-L$ set for a DEM grid point is the set of all elevation angles (θ) between that point and each of the grid points (filled circles in Figure 1) located on a profile along an azimuth D and within radial distance L . The largest θ in the $D-L$ set, shown in Figure 3, is required to calculate elevation angles. By expressing the $D-L$ set as ${}_D S_L$, we introduce two quantities,



${}_D \beta_L$: the maximum elevation angle in the ${}_D S_L$

and

${}_D \delta_L$: the minimum elevation angle in the ${}_D S_L$.

These angles, the minimum angles of elevation or depression, respectively, for which the line-of-sight is unobstructed out to a specified range (here L), are the *mask angles* of the military tactician (Wood, 1963; Anon., 1990). These two angles, which also are involved in the calculation of terrain viewsheds (Lee, 1994; Fisher, 1996), enable us to define the next quantity.

Definition 2: The *zenith angle* at a DEM grid point along azimuth D within radial distance L is

$${}_D \phi_L = 90 - {}_D \beta_L \quad (3)$$

and the *nadir angle*

$${}_D \psi_L = 90 + {}_D \delta_L \quad (4)$$

As illustrated in Figure 3, the zenith angle ${}_D \phi_L$ is the maximum vertical angle subtended by a selected grid point and any of the points viewed from above the surface along a chosen azimuth D up to distance L . The corresponding nadir angle ${}_D \psi_L$ for that point is the maximum angle subtended by the chosen point and any other point viewed from below the surface along azimuth D within L . Like terrain mask-angles, ${}_D \phi_L$ and ${}_D \psi_L$ thus depend both upon the configuration of the surface surrounding the point of interest and upon the specified range L within which points are considered. Moreover, because ${}_D S_L$ computed within increasingly large distances L includes more grid points, but not necessarily a commensurate increase in terrain relief, both ${}_D \phi_L$ and ${}_D \psi_L$ tend to diminish with increasing L .

Openness

We obtain surface openness by calculating either zenith or nadir angles for all eight compass directions from the central point A (double circled in Figure 1) and taking the mean.

Definition 3: *Positive openness* Φ_L at a location on a surface within the distance of L on the DEM is

$$\Phi_L = (\phi_L + {}_{45}\phi_L + \dots + {}_{315}\phi_L)/8 \quad (5)$$

and *negative openness* Ψ_L within a distance L is

$$\Psi_L = (\psi_L + {}_{45}\psi_L + \dots + {}_{315}\psi_L)/8. \quad (6)$$

Positive openness at a DEM grid point A is the average of *zenith* angles subtended by A and the optimal point (that yielding the highest angle) viewed *above* the surface along each of the eight azimuths D_{0-315} —up to the specified distance L (Figure 3). Similarly, *negative openness* averages the eight *nadir* angles subtended by point A and the optimal point viewed *below* the surface along azimuths D_{0-315} within L . To forestall possible confusion, we note that values of Φ_L and Ψ_L always take the positive sign. Openness is designated “positive” and “negative” to avoid the awkward terminology cited in the next paragraph. We adopt this “positive”/“negative” convention in the same sense as has been used to express terrain-slope curvature (Pike, 1988), which also takes only positive values (positive curvature is convex-upward; negative curvature is concave-upward).

Positive, or “above-ground,” openness Φ_L at a grid point is constrained by surrounding topography and thus is an angular estimate of the 360° horizontal extent of area around the point. We originally conceptualized the measure as “openness of the terrain to the sky.” Its negative counterpart, “below-ground” openness Ψ_L —less helpfully verbalized as openness *per se*—is the corresponding angular measure of 360° spatial extent around the central grid point. Figure 4, which shows these two measures schematically for angles < 90°, represents openness as the largest right cone of specified base diameter $2L$ that can be fit to a point on a DEM. Comparable representations of Φ_L and $\Psi_L > 90^\circ$ are impossible-to-illustrate constructs in topology (e.g., Barr, 1964) that are better rendered in two dimensions, as in Figures 5A and 5D. Figure 4 is a simplification of the true figure of merit, because the base of the conical figure actually fit to the terrain rarely will be a perfect circle of diameter $2L$. As shown in Figure 6, the base will have an irregular, commonly elongate and eccentric, form that necessarily varies with the elevation angles determined along the eight azimuths.

Like its constituent individual zenith (ϕ_L) and nadir (ψ_L) angles, the corresponding mean values of openness Φ_L and Ψ_L also are constrained to decrease with increasing range L . Accordingly, the choice of L will emphasize topography at different length scales. Larger values of L will highlight larger features, and smaller L smaller forms.

Discussion

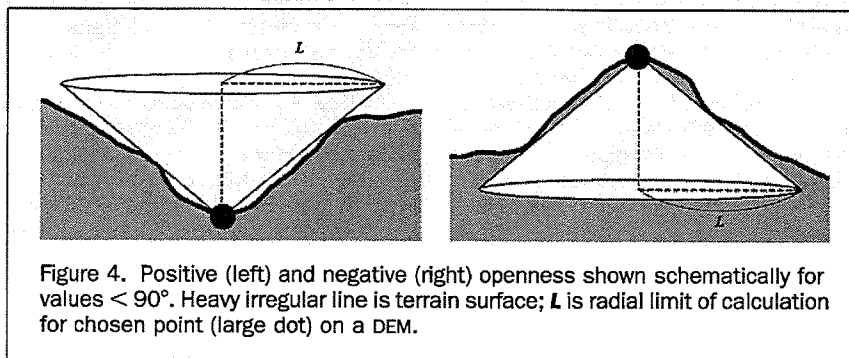
Openness expresses a topographic attribute that possibly is captured by no other measure or combination of them,

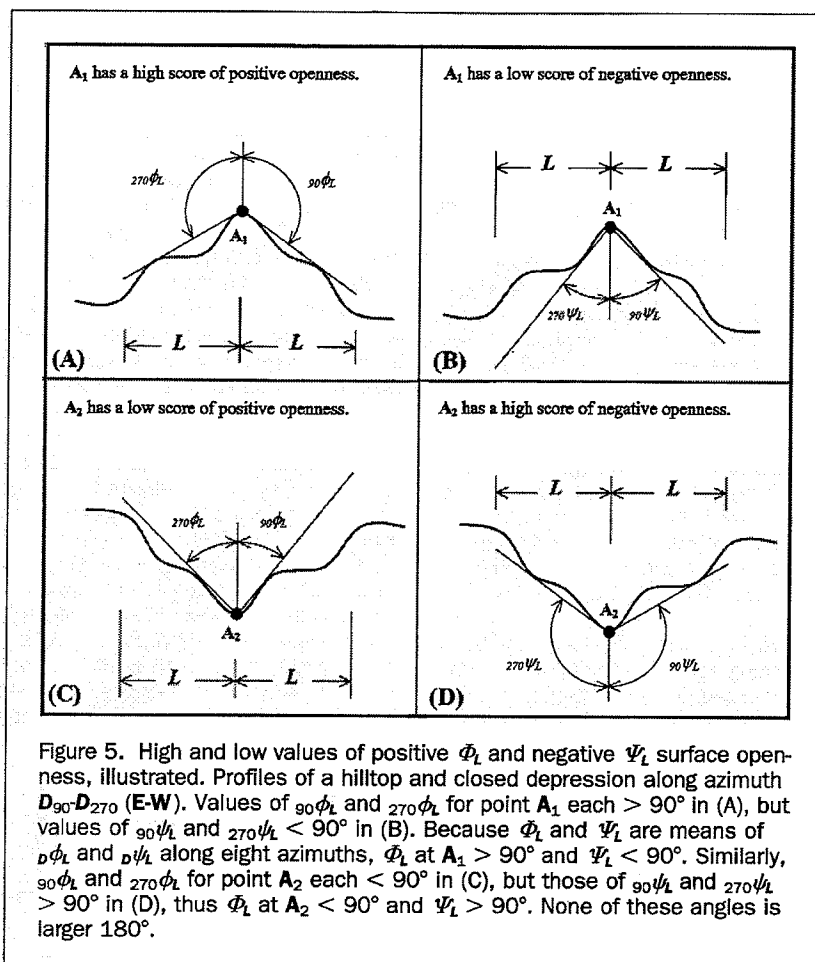
although this remains to be tested against parameters that describe terrain fabric (Pike *et al.*, 1989; Guth, 2001). The characteristic appears to be the degree of geometric “dominance” of one location on a surface by another. This parameter expresses two configurations commonly encountered in the landscape: command of an expanse of terrain by one or several elevated relief features (positive openness Φ_L), and the degree of “enclosure” of a lower location by elevated surroundings (negative openness Ψ_L). As such, openness is sensitive to the local relief: distance conditions that express much of an area’s topographic distinctiveness (Pike *et al.*, 1989).

The range of contrasts is illustrated by profiles of a hilltop and a closed depression along the azimuth D_{90° – D_{270° (Figure 5). If the center point of an openness calculation is on a summit rising above its surroundings and flanked by steep slopes, the resulting values of ${}_{90}\phi_L$ and ${}_{270}\phi_L$ will exceed 90° (Figure 5A), as will positive openness Φ_L , which is the average of eight values of ϕ_L . Summits and ridge lines thus will appear on a plot of Φ_L as, respectively, compact and linear groupings of high-scoring cells. Commensurately, a negative-openness calculation at the same location (Figure 5B) would yield low values of ${}_{90}\psi_L$ and ${}_{270}\psi_L$, < 90°, and summits and ridge lines on a plot of Ψ_L will be groups of low-scoring cells. Topographic features that result in neither high nor low values of Φ_L and Ψ_L yield groupings of intermediate-scoring cells. Taking the inverse example, if the center point of an openness calculation lies within a depression surrounded by steep slopes (Figure 5C), the resulting value of positive openness Φ_L will be less than 90 degrees. Topographic lows, therefore, will appear on maps of Φ_L as groups of low-scoring cells. However, that same depression will generate a high value of negative openness $\Psi_L > 90^\circ$ (Figure 5D). Topographic depressions and valley lines thus will show up on a L plot as clusters and strings of high-scoring cells.

The closed-depression example, which is the approximate inverse of the summit example, raises an intriguing point. Figure 5 would at first appear to show that negative openness is redundant: that simply subtracting Φ_L from 180° would be equivalent to Ψ_L , but this is not so. The two quantities differ substantially, due to irregularity of the ground surface surrounding point A . It is for this reason that negative openness Ψ_L emphasizes concave features (Figure 5D) more crisply in gray-tone images (Figures 7 through 13 below) than does $180^\circ - \Phi_L$ (Figure 5C). Otherwise, $180^\circ - \Phi_L$ would suffice to capture depressions and valleys and there would be no need for Ψ_L .

The correspondence of openness to terrain configuration is illustrated in Figure 6 by octagonal plots that compare *zenith* and *nadir* angles, along the eight azimuths, for nine test surfaces. Among these simple models are all the important elements of topography—plain, slope, summit, depression, ridge, valley, and saddle (Maxwell, 1870). Depending on shape of the ground, angular values of ϕ_L and ψ_L increase with distance outward from the center of each figure, up to range L . Openness is equivalent to the area of the octagon projected at L . Because





features in natural terrain are complex composites of these basic elements, the set of eight angles that comprise openness will vary considerably with location of the point of origin and character of the surrounding topography. A grid point in highly irregular terrain thus will generate a variety of constituent angles and a correspondingly distorted octagonal pattern. The angular plots in Figure 6 constitute a kind of geometric signature of topographic form; openness also could be part of a more complex, multivariate signature (Pike, 1988).

Examples and Applications

While we defer the application of corresponding values of openness as an analytical parameter—for example, as a constituent of a geometric signature—to a later experiment, in this paper we exemplify the visualization counterpart of terrain modeling by several maps of surface openness. These few selections represent a variety of terrains, map scales, L -values, and DEM sources and resolutions. Not all possible combinations of these applications are shown. In order to highlight both terrain convexities and concavities, for example, values of positive openness and negative openness must be compiled as separate maps of the same area. Also, separate openness maps of the same area can be computed for different values of L , to emphasize fine- or coarse-scale features.

As in mapping elevation, slope, and shaded relief calculated from DEMs, tones of gray are assigned to values of openness within a range that produces an image with optimal detail and contrast. The convention adopted for our images is that customarily followed for elevation and slope: high values of

openness are represented by light tones and low values by dark tones. Accordingly, images of positive openness ϕ_L , which are designed to highlight topographic convexities, show ridges as bright lines and rivers and other elongate concavities as dark lines, whereas maps of negative openness ψ_L emphasize drainages (light tones) at the expense of mountains and other convex-features (dark tones). Intermediate values of both parameters yield gray tones. Although we experimented with reversing this tonal convention, we chose the standard scheme on aesthetic and intuitive grounds—the resulting images simply look more pleasing to the eye and seem easier to interpret. Mapping openness values carries some perceptual consequences. While openness images superficially resemble raster-based maps of elevation, shaded relief, or slope, their appearance can be deceiving at first. Individuals familiar with the more conventional types of digital maps may require some acclimation to openness images before viewing them becomes intuitive.

Maps of positive openness in Figures 7 and 8, computed at different values of L , illustrate various features of stratovolcanoes on the main Japanese island of Honshu (Yoshikawa *et al.*, 1981, p. 81–87). Landforms in the vicinity of Mt. Fuji in south-central Honshu (Figure 7) that are easily recognized from openness textures include aligned low hummocky hills formed in flank eruptions prior to 1707 (light-toned area, center). Steep ridges in much of the image appear as bright thin lines; old lava flows on Fuji and the more gently sloping ridges on the eroded Mt. Ashitaka volcano and Hakone caldera to the Southeast are less distinct. The area around Mt. Chokai in

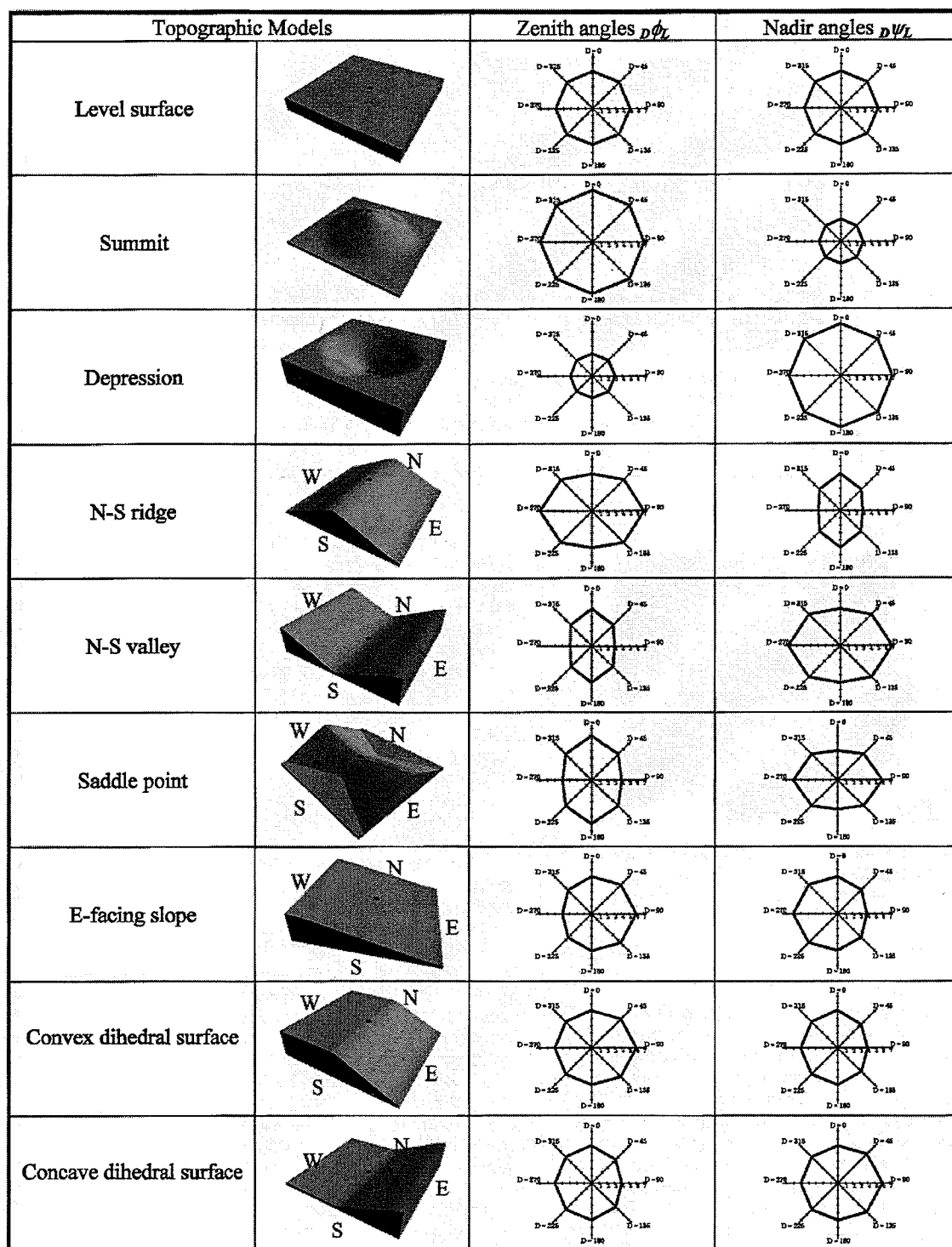


Figure 6. Variation in surface openness. Differing values of the eight zenith angles ${}_D\phi_L$ and nadir angles ${}_D\psi_L$, at a DEM grid point (black dot), for nine simple terrains. Positive and negative openness ϕ_L and ψ_L are proportional to the area enclosed by the octagonal plots of ${}_D\phi_L$ and ${}_D\psi_L$, respectively. Evenly-spaced numbers 1 through 7 along azimuths are for comparison purposes and do not correspond to actual angles; range L for all calculations = 7.

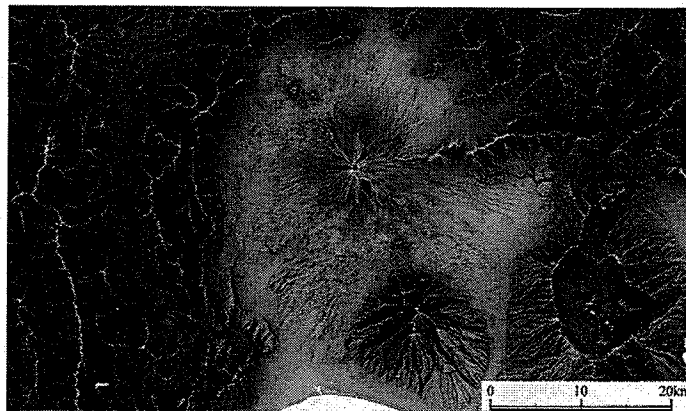


Figure 7. Positive openness ($L = 5$ km) for the Mt. Fuji area, southern Honshu (N35:06:24 - N35:31:42, E138:18:07 - E139:09:16) computed from a 50-m DEM of the Geographical Survey Institute of Japan (GSJ).



Figure 8. Positive openness ($L = 1$ km) for Mt. Chokai, northern Honshu (N38:43:41 - N38:59:32, E139:44:49 - E140:14:56) computed from a 10-m DEM from the Hokkaido Map Company (HMC).

northwest Honshu (Figure 8), rendered at one-fifth the value of L in Figure 7, is more detailed and also differs in morphology from the area around Mt. Fuji. The recent growth process of the volcano, clearly evident in the lobate form of its many fresh lava flows, is well illustrated by positive openness.

Figures 9 and 10 contrast two non-volcanic terrains in Japan in maps of negative openness that emphasize topographic concavities at very different values of L . The Tohka-machi area (Figure 9), located in the upper reaches of the Shinano River in north-central Honshu, exemplifies variation in the patterns of valleys as well as in the layers of sediment in the main valley. Figure 10 shows the Tohno area, east of Mt. Chokai. The distinctly reticular structure of this terrain, at one-tenth the L used to compute Figure 9, reflects small stream channels that developed along planes of weakness caused by jointing in the underlying granite bedrock. Because the area is densely vegetated, the macroscopic structure of this joint pattern had remained unknown to geologists and is shown clearly here for the first time (Kanisawa and Yokoyama, 1999). More variety of topographic features can be observed in the openness maps of Japan (Yokoyama, 2001), which were generated from a 50-m interval DEM with $L = 5$ km and printed at a scale of 1:50,000.

Figures 11 and 12, showing positive and negative openness at the same L -value for a small area 50 km south of San Francisco in California's coastal Santa Cruz Mountains, are excerpted from two large openness maps of the entire ten-county San Francisco Bay region (not shown). Most of this rough terrain lies within the La Honda 7.5-minute quadrangle, the first topographic map published by the U.S. Geological Survey in which a contour-to-grid technique replaced photogrammetric scanning to create a higher quality 30-m DEM (Pike *et al.*, 1987). The crisp valleys and ridge lines in Figures 11 and 12, respectively, reflect the region's strong contrasts in rock type (Pike *et al.*, 1988) as well as the imprint of recent tectonic uplift and consequent erosion. The steep terrain is subject to chronic debris-flow (landslide) activity during the rainy California winter and thus is thinly populated.

The lofty topography of Tibet and the high-relief Himalaya Range are attracting fresh scientific interest (Fielding *et al.*, 1994; Albright *et al.*, 1998; Zeitler *et al.*, 2001). Figure 13, a negative openness map of this large region, emphasizes the hydrology of the southern Tibetan Plateau and its relation to the Himalayas. The distinctive north-south valleys were carved through the rising mountains by rivers draining the plateau. The contrasting rectangular areas reflect differences in the source and quality of data in the GTOPO30 DEM. This contrast is an important feature of the openness parameter. The large map of negative openness (not shown) containing the California sample in Figures 11 and 12 also revealed an imperfect match between two source DEMs—suggesting that the openness is an excellent tool for performing quality control on regional DEMs mosaicked from several smaller data sets.

Application of openness need not be limited to the portrayal and interpretation of Earth's landscapes. Like shaded-relief mapping, openness mapping is an image-processing technique capable of representing surface features anywhere a DEM exists or can be prepared—Earth's seafloor (Smith and Sandwell, 1997) and surfaces of the solid planets and satellites (Smith *et al.*, 1999). Finally, the technique is not restricted to natural landscapes. Digital terrain modeling has an important micro- and nano-scale counterpart in *surface metrology*, the numerical characterization of industrial surfaces—such as magnetic tape and disk surfaces and automobile-engine cylinder walls (Pike, 2000; Pike, 2001). Metrology recently was revolutionized by its ability to create and manipulate square-grid height matrices that are fine-scale analogs of DEMs. Because the

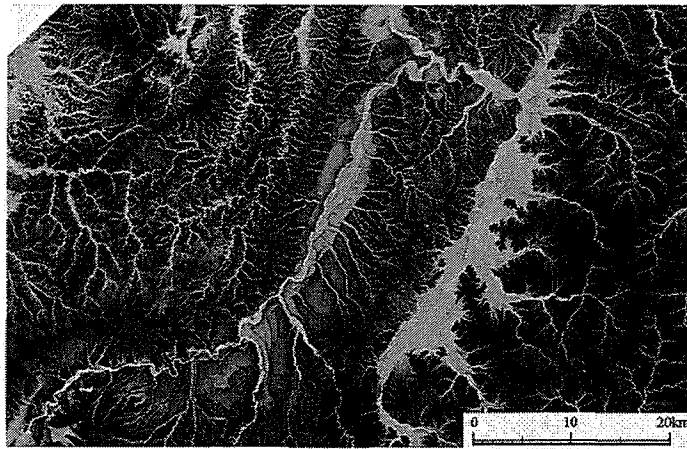


Figure 9. Negative openness ($L = 5$ km) for the Tohka-machi area, central Honshu (N36:54:07 - N37:19:20, E138:21:58-E139:09:05) computed from the 50-m GSJ DEM.

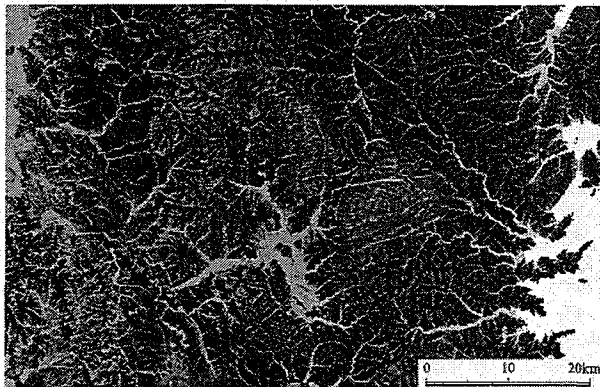


Figure 10. Negative openness ($L = 500$ m) for Tohno area, central Honshu (N39:11:00 - N39:36:41, E141:09:58 - E142:01:06) computed from a 10-m DEM from HMC.

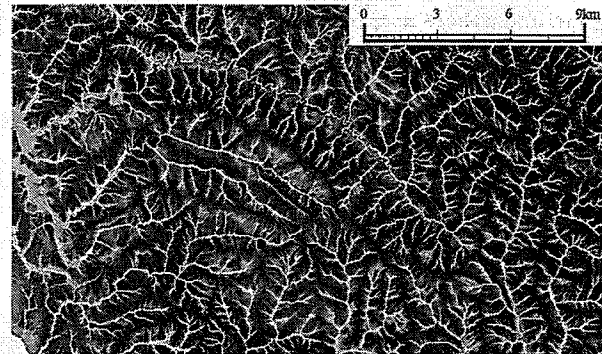


Figure 12. Negative openness ($L = 500$ m) for the area in Figure 11.

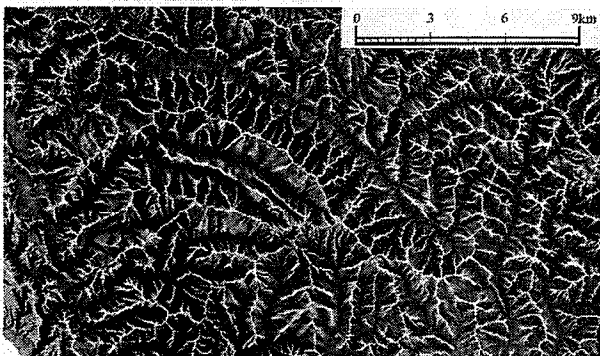


Figure 11. Positive openness ($L = 500$ m) for an area south of San Francisco, California (N37:10:03 - N37:17:43, W122:06:01 - W122:22:1) computed from a 30-m DEM of the U.S. Geological Survey (USGS).

surface topography of manufactured components is routinely modeled by the same techniques of parameterization and visualization as used in the Earth sciences, we suggest that the concept of surface openness offers a new tool for metrologic applications as well.

Conclusion

A new image-processing technique generates an angular measure of surface form, here termed *openness*, that visualizes the topographic dominance or enclosure of any location on an irregular surface represented by a DEM. The measure incorporates the terrain line-of-sight (viewshed) principle and is calculated from zenith and nadir angles along eight DEM azimuths. Openness is expressed in two modes. Positive openness emphasizes convex features of topography and negative openness concave features. Values of openness, which are shown as gray-scale maps resembling shaded-relief images, are independent of the position of any light source and less sensitive to noisy DEMs than are other parameters. Different topographic features can be emphasized by tailoring a radial sampling distance to the scale of the selected area. Openness maps not only create new possibilities for geomorphological and geographical

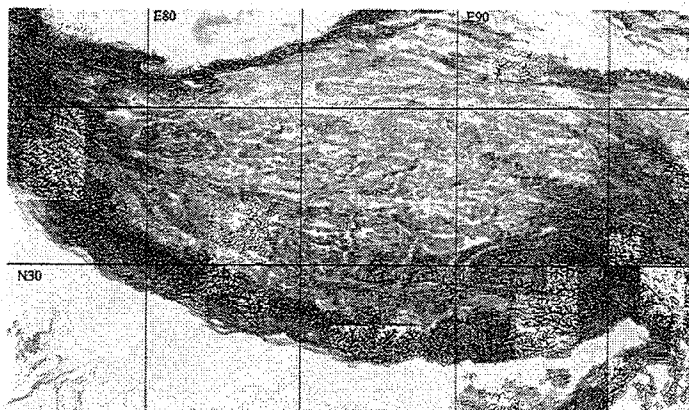


Figure 13. Negative openness ($L = 5$ km) of the Tibetan Plateau and Himalaya (N25:06:30 - N38:14:00, E75:30:30 - E97:49:00) computed from a 1-km GTOPO30 DEM available from the USGS.

interpretation, but also are suited to visualization of the Earth's seafloor, planetary landforms, and features on any irregular surface, including those micro- and nano-landscapes created by manufacturing processes.

Acknowledgment

We thank Peter Guth and Ralph Haugerud for comments on an earlier version of this paper.

References

- Albright, T.P., T.H. Painter, D.A. Roberts, J. Shi, J. Dozier, and E. Fielding, 1998. Classification of surface types using SIR-C/X-SAR, Mount Everest Area, Tibet, *Journal of Geophysical Research*, 103(E11):25823–25837.
- Alpha, T.R., and R.E. Winter, 1971. Quantitative physiographic method of landform portrayal, *Canadian Cartographer*, 8(2):126–136.
- Anonymous, 1990. *Firefinder Mask Considerations, Tactics, Techniques, and Procedures for Field Artillery Target Acquisition*, FM 6-121, Appendix F, Headquarters, Department of the Army, Washington, D.C., 5 p. <http://www.adtdl.army.mil/cgi-bin/atdl.dll/fm/6-121/appf.pdf>.
- Barr, S., 1964. *Experiments in Topology*, Crowell, New York, N.Y., 210 p. (reprinted 1989, Dover Publications, New York, N.Y.)
- Blaszczynski, J.S., 1997. Landform characterization with geographic information systems, *Photogrammetric Engineering & Remote Sensing*, 63(2):183–191.
- Carter, J.R., 1992. The effect of data precision on the calculation of slope and aspect using gridded DEMs, *Cartographica*, 29(1):22–34.
- ESRI, 1992. *Cell-Based Modeling with GRID 6.1. ARC/INFO User's Guide, Supplement—Hydrologic and Distance Modeling Tools*, Environmental Systems Research Institute Inc., Redlands, California, variously paged.
- Evans, I.S., 1972. General geomorphometry, derivatives of altitude and descriptive statistics, *Spatial Analysis in Geomorphology* (R.J. Chorley, editor), Harper and Row, New York, N.Y., pp. 17–90.
- Fielding, E.J., B.L. Isacks, M. Barazangi, and C.C. Duncan, 1994. How flat is Tibet? *Geology*, 22(2):163–167.
- Fisher, P.F., 1996. Extending the applicability of viewsheds in landscape planning, *Photogrammetric Engineering & Remote Sensing*, 62(11):1297–1302.
- Guth, P.L., 2001. Quantifying terrain fabric in digital elevation models, *The Environmental Legacy of Military Operations* (J. Ehlen and R.S. Harmon, editors), Geological Society of America Reviews in Engineering Geology, 14, chap. 3 (in-press).
- Horn, B.K.P., and M.J. Brooks (editors), 1989. *Shape from Shading*, M.I.T. Press, Cambridge, Massachusetts, 577 p.
- Imhof, E., 1965. *Kartographische Geländedarstellung*, Walter de Gruyter, Berlin, Germany, 425 p.
- Jenson, S.K., and J.O. Domingue, 1988. Extracting topographic structure from digital elevation data for geographic information systems analysis, *Photogrammetric Engineering & Remote Sensing*, 54(11):1593–1600.
- Kanisawa, S., and R. Yokoyama, 1999. Extraction of geologic information from digital elevation map of 50m-mesh—Application of slope and openness maps to the Kitakami Mountains, *Chisitsu News*, (542):31–38 (in Japanese).
- Lee, J., 1994. Digital analysis of viewshed inclusion and topographic features on digital elevation models, *Photogrammetric Engineering & Remote Sensing*, 60(4):451–456.
- Mark, R.K., 1992. *A Multidirectional, Oblique-Weighted, Shaded-Relief Image of the Island of Hawaii*, U.S. Geological Survey Open-file Report 92-422, U.S. Geological Survey, Reston, Virginia, 3 p.
- Maxwell, J.C., 1870. On hills and dales, *The London, Edinburgh, and Dublin Philosophical Magazine and Journal of Science*, 40 (4th Series, July-Dec., No. 269):421–427.
- Moore, J.G., and R.K. Mark, 1992. Morphology of the island of Hawaii, *GSA Today*, 2(12):257–259 and 262.
- Peucker, T.K., and D.H. Douglas, 1975. Detection of surface-specific points by local parallel processing of discrete terrain elevation data, *Computer Graphics and Image Processing*, 4(4):375–387.
- Pike, R.J., 1988. The geometric signature—Quantifying landslide-terrain types from digital elevation models, *Mathematical Geology*, 20(5):491–511.
- , 2000. Nano-metrology and terrain modelling—Convergent practice in surface characterisation, *Tribology International*, 33(9):593–600.
- , 2001. Digital terrain modeling and industrial surface metrology—Converging realms, *The Professional Geographer*, 53(2):263–274.
- Pike, R.J., W. Acevedo, and D.H. Card, 1989. Topographic grain automated from digital elevation models, *Proceedings, Ninth International Symposium on Computer-Assisted Cartography*, 02–07 April, Baltimore, Maryland (American Society for Photogrammetry and Remote Sensing—American Congress on Surveying and Mapping), pp. 128–137.
- Pike, R.J., W. Acevedo, and G.P. Thelin, 1988. Some topographic ingredients of a geographic information system, *Proceedings, International Geographic Information Systems Symposium*, 15–18 November, Arlington, Virginia (NASA, Washington, D.C.), 2:151–164.

PAPER

Representation of topographical features by opennesses

Ryuzo YOKOYAMA*, Michio SIRASAWA*, and Yu KIKUCHI*

Abstract: Overground-openness and underground-openness are defined for a grid point on digital elevation models. The former is a characteristic quantity to describe sky extent over the point within a distance L and takes large values for convex landforms. The latter is to describe underground extent and takes large values for concave landforms. These concepts are applied to 50m-mesh digital elevation model of Mt. Iwate to make openness maps of $L = 5$ km and $L = 0.5$ km. The maps were found useful to represent topographical features such as the lines of ridge and valley.

**Department of Computer Science, Iwate University*

"Photogrametric Engineering and Remote Sensing" Vol. 38, No. 4, pp. 26-34, 1999

1. Introduction

Diffusion of digital elevation model has allowed effective topographic representation and analysis by computer. As a method of displaying a topographic map with an appearance of solidity, there has been known from old times a technique of relief map by a hill shading method. This is a method of indicating slopes facing a light source, brightly, and indicating slopes with the light source in the background, darkly. Although manually produced relief maps were subject to limitations in accuracy and reproducibility, now with mathematically systematized procedures for preparation of a relief map from a digital elevation model, it is allowed to prepare various ones as necessary for the use^{1, 2)}. In the relief map, changes in terrain crossing an arrival direction of light can be clear represented, but changes in terrain parallel to the arrival direction of light become unclear. On the other hand, there have been methods proposed for extraction of a variety of topographic features (ridgeline, valley line, gradient, valley density, water catchment area, etc.) from a digital elevation model³⁻⁶⁾. However, most of their algorithms have been based on a local calculation by elevation values in a vicinity of a site, susceptible to noises, and unable to grasp comprehensive topographic features, as shortcomings.

This paper introduces a concept of "openness", to propose a new technique for representation of topographic features based on a digital elevation model. Viscerally, the

openness is a quantification of a degree by which the site is projected on the earth in comparison with peripheral, or a degree by which the site is cut belowground. Mapping the openness permits extraction of information suitable to a topographic scale depending on a specified calculation distance, allowing for a representation free of orientation or local noise. Actually, openness maps of areas around Mt. Iwate were prepared on the basis of a “numerical map 50m-mesh (elevation)” issued by the Geographical Survey Institute of Japan, revealing that the present technique is particularly excellent in extraction of ridgelines and valley lines, allowing wealth of topographic and geologic information to be made out.

There will be described in Chapter 2 the “numerical map 50m-mesh (elevation)”, and in Chapter 3, the openness will be defined. In Chapter 4, prepared openness maps will be discussed. Chapter 5 provides a conclusion.

2. Preparation of a digital elevation model by UTM coordinate system

The “numerical map 50m-mesh (elevation)” is a two-dimensional array of elevations, read at intervals of 10 cm, at centers of meshes (mesh intervals being 2.25 seconds in the latitudinal direction, and 1.50 seconds in the longitudinal direction) equally dividing the height and the width of a 1/25,000 terrain map. In the “numerical map 50m-mesh (elevation)”, the distance between sample points (as positions where elevations are read) varies depending on the longitude and latitude (for example, on a northern latitude line of 40 degrees, relative to the north-south direction where it is 46.26 m in, it becomes 53.37 m in the east-west direction), in addition to that arrayed directions of sample points are disaccord with azimuths, except for the north-south, such that the greater the distances the greater the differences.

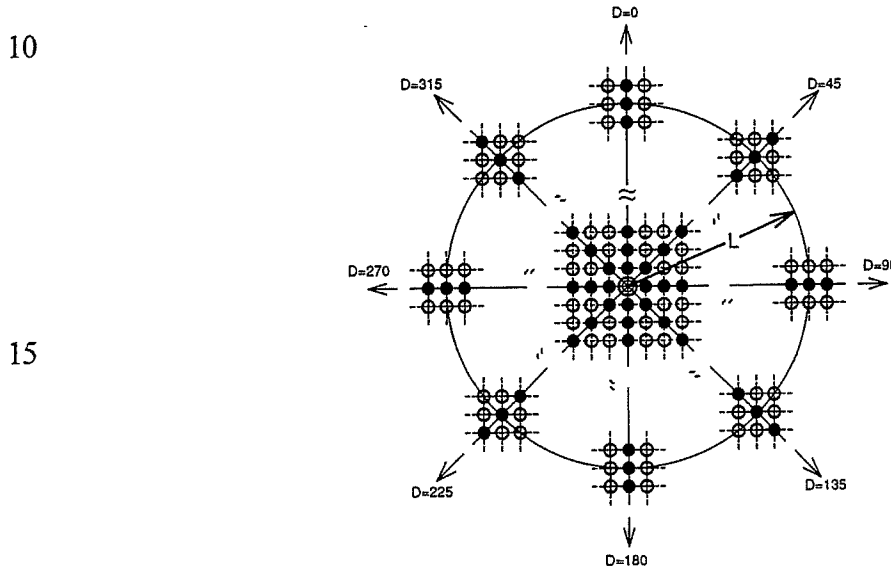
For a convenient topological analysis over a wide area, the digital elevation model should have sample points at a constant spacing, and data array directions in accord with azimuths. Hence, based on the “numerical map 50m-mesh (elevation)”, we prepared a set of digital elevation data by an UTM projection (in application of Zones 52 to 55) having a sample point spacing of 50 m. This will be referred to as “UTM-DEM”. For conversion from the “numerical map 50m-mesh (elevation)” to the UTM-DEM, there was employed a conformal first-order interpolation⁷⁾.

Fig. 1 illustrates an arrangement of sample points in the UTM-DEM. As the azimuth is

defined in terms of a clockwise angle D relative to the north to be 0 degrees, there are eight azimuths (north, northeast, east, south east, south, southwest, west, north west) appearing in sequence with respect to each 45 degrees from 0 degrees. Hereinafter, a single sample point will be described by

5 (i, j, H)

where i and j are numbers of a row and a column indicating a position of the sample point, and H is the elevation.



20 Fig. 1: Sample points arrayed about a focused sample point (with a double circle mark) in the UTM-DEM, in which black circle marks are sample points along the eight azimuths, and white circle marks are sample points else.

3. Overground openness and underground openness

25 All the following discussions presuppose the UTM-DEM.

3.1 Overground angle and underground angle

Suppose two sample points $A (i_A, j_A, H_A)$ and $B (i_B, j_B, H_B)$. For the sampling at intervals of 50 m, the A and B have a distance in between, such that

30
$$P = 50\sqrt{(i_A - i_B)^2 + (j_A - j_B)^2}$$

Fig. 2 illustrates a relationship between sample points A and B, with an elevation of 0 m as a reference. The sample point B has an elevation angle θ with respect to the sample point A, to be given such that

$$\theta = \tan^{-1}\{(H_B - H_A)/P\}$$

5 where θ has a sign to be: ① positive for $H_A < H_B$; or ② negative for $H_A > H_B$.

10

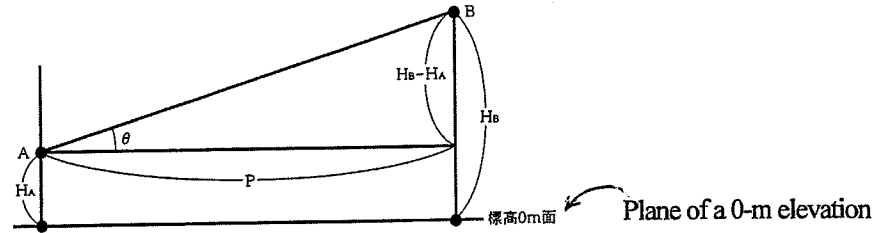


Fig. 2: Elevation angle θ of a sample point A with respect to a sample point B

15

With respect to a focused sample point, a set of sample points along an azimuth D within a range of a distance L is described by ${}_D S_L$, which will be referred to as “D-L set of the focused sample point”.

Now (referring to Fig. 3), letting

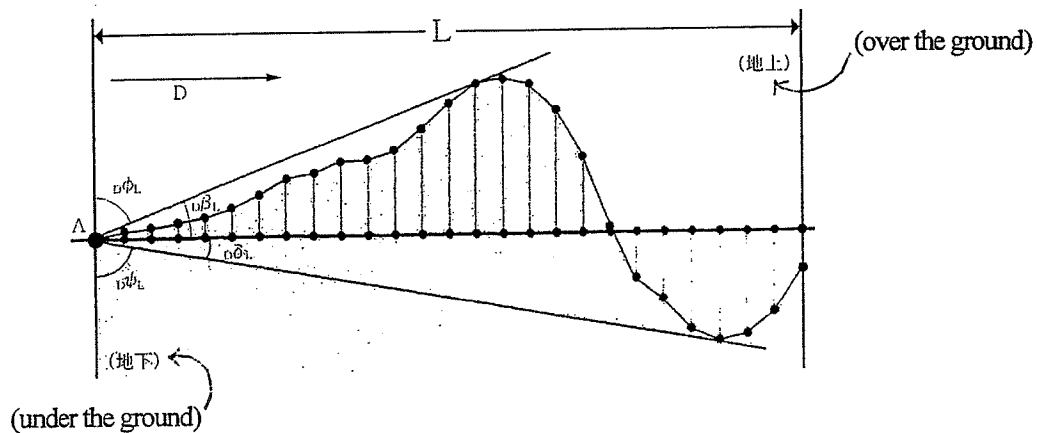
${}_D \beta_L$: the maximum among elevation angles of set elements of a ${}_D S_L$ of a focused sample point, and

20

${}_D \delta_L$: the minimum among elevation angles of set elements of a ${}_D S_L$ of a focused sample point,

a definition is made, as follows:

25



30

Fig. 3: Overground and underground angles of a D-L set of a focused sample point A.

Definition I: With respect to a D-L set of a focused sample point, an overground angle and an underground angle mean

$${}_D\phi_L = 90 - {}_D\beta_L,$$

5 and

$${}_D\Psi_L = 90 + {}_D\delta_L,$$

respectively.

${}_D\phi_L$ means the maximum of a zenithal angle by which a sky along an azimuth D is visible within a range of distance L from a focused sample point. What they call skyline angle corresponds to the zenithal angle, as the L is set infinite. And, ${}_D\Psi_L$ means the maximum of a nadir angle by which a nadir along an azimuth D is visible within a range of distance L from a focused sample point. For an increased L, the number of sample points belonging to the ${}_DS_L$ is increased, so the ${}_D\beta_L$ has a non-decreasing characteristic with respect to L, while the ${}_D\delta_L$ has a non-increasing characteristic, vice versa. Accordingly, both ${}_D\phi_L$ and ${}_D\Psi_L$ have a non-increasing characteristic with respect to L.

In the surveying, the elevation angle is a concept defined to a horizontal plane as a reference passing a focused sample point, and does not strictly accord with θ . Further, for strict discussions of the overground and underground angles, also a curvature of the earth should be considered, so the definition I is not always an exact description. The definition I is a concept defined absolutely assuming the use of a UTM-DEM for topographic analysis.

3.2 Overground openness and underground openness

The overground angle as well as the underground angle is a concept with respect to a specified azimuth D, which is now extended to introduce a definition, as follows.

Definition II: For a distance L with respect to a focused sample point, an overground openness and an underground openness mean

$$\Phi_L = ({}_0\phi_L + {}_{45}\phi_L + {}_{90}\phi_L + {}_{135}\phi_L + {}_{180}\phi_L + {}_{225}\phi_L + {}_{270}\phi_L + {}_{315}\phi_L) / 8$$

and

$$\Psi_L = ({}_0\Psi_L + {}_{45}\Psi_L + {}_{90}\Psi_L + {}_{135}\Psi_L + {}_{180}\Psi_L + {}_{225}\Psi_L + {}_{270}\Psi_L + {}_{315}\Psi_L) / 8,$$

30 respectively.

The overground openness represents an extent of sky visible within a range of distance L from a focused sample point, and the underground openness represents an extent of nadir within a range of distance L , when looking under the ground, standing on the head (refer to Fig. 4 [overleaf]).

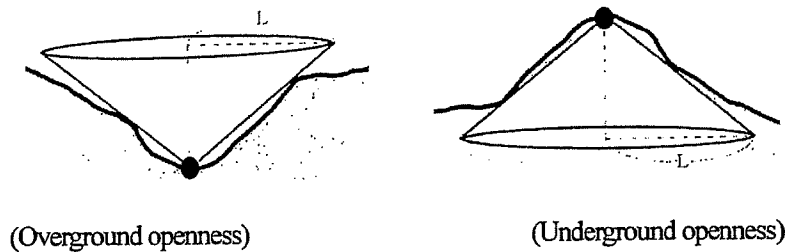

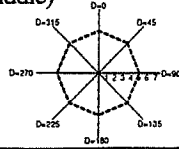
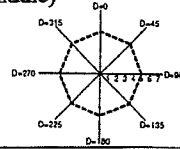

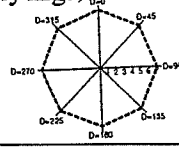
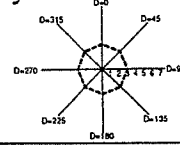

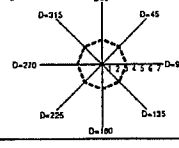
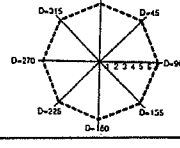

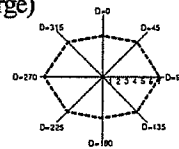
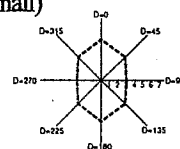

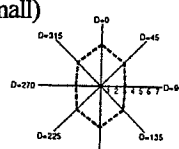
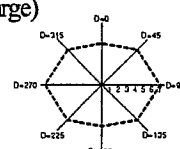

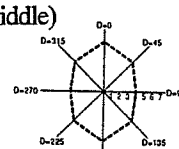
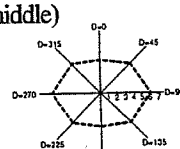

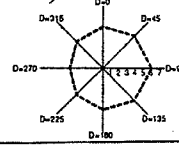
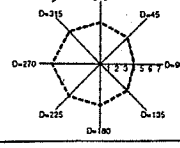

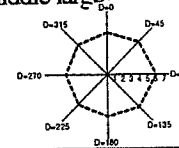
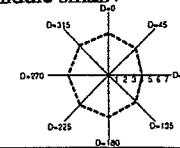
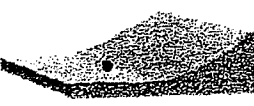
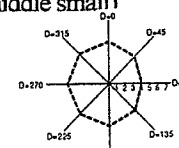
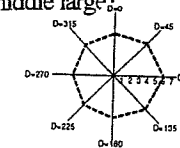


Fig. 4: Opennesses at a focused sample point (marked with a black circle)

The opennesses depend on the distance L and a peripheral terrain. Listed in Table 1 are sets of azimuth-wise octagonal plots of overground angles and underground angles representing overground opennesses and underground opennesses of nine fundamental topographic forms. Generally, the higher a site is projected from around the greater the overground openness becomes, so the value is large on a peak or ridge, and small in a dent or valley floor. To the contrary, the lower a site is cut underground the greater the underground openness becomes, so the value is large in a dent or valley floor, and small on a peak or ridge. Really, there are various mixtures of fundamental topographic forms even within a range of distance L , giving various combinations of values to sets of octagonal plots of overground angles and underground angles.

Table 1: Overground opennesses and underground opennesses of focused sample points (marked with black circles) on nine fundamental topographic forms, represented by sets of octagonal plots on azimuth-wise relative scales calibrated with five graduations to opennesses of overground and underground angles of flatland (to be 90 degrees).

	Fundamental topographic forms		Overground opennesses	Underground opennesses
1	Flatland		(middle) 	(middle) 
2	Mountaintop		(very large) 	(very small) 
3	Depression		(very small) 	(very large) 
4	Ridge extending North-South		(large) 	(small) 
5	Valley extending North-South		(small) 	(large) 
6	Col between E-W valley and N-S ridge		(middle) 	(middle) 
7	Uniform slope facing East		(middle) 	(middle) 
8	Boundary between western flatland and eastern down-slope		(middle large) 	(middle small) 
9	Boundary between western flatland and eastern up-slope		(middle small) 	(middle large) 

4. Openness maps prepared

For an area about Mt. Iwate, between latitudes 39 degrees 36 minutes and 39 degrees 57 minutes north and between longitudes 140 degrees 44 minutes and 141 degrees 23 minutes east, openness maps of $L = 5$ km and $L = 0.5$ km were prepared. An operational processing by Laplacian also was performed for a comparison purpose.

4.1 Topographic features of target area

Fig. 5 is a chorography of the target area. Mt. Iwate (2,038 m) is substantially centered, with Shizukuishi Basin at the southern foot. At the eastern foot, there is a flatland extending as upstream part of Kitakami River. At east of the flatland, there are closing mountains in western part of Kitakami Highlands about Mt. Himegami (1,124 m). Further, there is Ohu' Range of Mountains at the west of Mt. Iwate, with volcanic terrain formed along a district between Hachimantai (1,613 m) and Akita-komagatake (1,637 m), and in the southern west part, with non-volcanic terrain spread about Gobanmori (1,048 m).

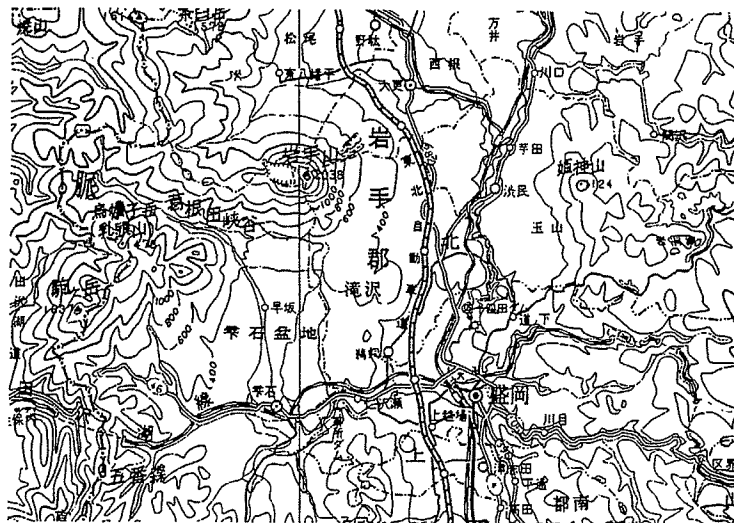


Fig. 5: Target area of prepared openness maps (between latitudes 39 degrees 36 minutes to 39 degrees 57 minutes north, and between longitudes 140 degrees 44 minutes to 141 degrees 23 minutes east)

4.2 5 km overground openness

Fig. 6 is an overground openness map for $L = 5$ km. The greater the openness the more white the indication, whereby tops and ridgelines extending from them appear as white, and valley lines, as black, while, among others, flatlands and slopes or such appear as intermediate gray tones. The more white a ridgeline the higher the latitudes in comparison with surroundings (within a range of calculation distance L), and the thinner it is the steeper the topographic form. Likewise, the darker a valley line the deeper the valley, and the thinner it is the narrower the valley floor. For the former, as a typical, there is a ridgeline extending from the top of Mt. Iwate, and for the latter, there is Kuzuneta Ravin extending along a southwest foot of Mt. Iwate. The district at the west side of Mt. Iwate is a typical shield volcanic (aspite) district forming a gentle slope, which is seen as a black-and-white patched texture. On the other hand, districts of Gobanmori along the southwest edge as well as Kitakami Highlands at the east form textures with featuring black and white lines, whereby it is found that they constitute an erosional topography with intersecting ridgelines and valley lines. It can be seen that, for Gobanmori, with great and rough black-to-white contrasts, the landform should have actively dissected steep and large undulations, and for Kitakami Highlands, with small and fine contrasts in texture, the landform should have small undulations. Flatlands in upstream part of Kitakami River and Shizukuisi Basin are flat, and those districts appear gray as a whole, while terraces as well as erosional landforms can be read when observed into details.

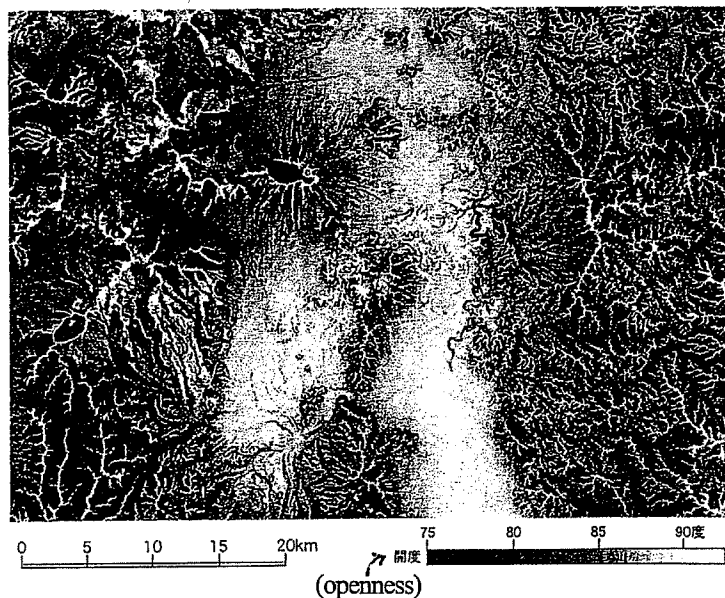


Fig. 6: Overground openness map for $L = 5$ km

4.3 5 km underground openness

Fig. 7 is an underground openness map for $L = 5$ km. The greater the openness the more white the indication. The deeper a valley the more white it is, and the wider the floor the bigger the valley appear. Even in those parts extending as relatively white regions, more white lines are visible, which are valley floors with advancing new dissections. Overground

5 lines are visible, which are valley floors with advancing new dissections. Overground

opennesses in Fig. 6 and underground opennesses in Fig. 7 have correspondence relationships, though representing topologic features from different points of observation, respectively. From the viewpoint that they are both easy to make out by white parts to be focused, we can say that

Fig. 6 is suitable to make out a topography mainly composed of ridgelines, and Fig. 7, suitable

10 to make out a topography mainly composed of valley lines. It may well be said that important topographic and geographic information on undulation, dissection, swelling, and the like are reflected in black-and-white textures of Fig. 6 and Fig. 7, i.e., in parts of lineated texture, such as, for lines, on the density, whether long or short, thick or thin, the degree of flexion, or the contrast, and in parts of patched texture, such as on the contrast, extent, or relationship of connection.

15 Fig. 6 and Fig. 7 exhibit comprehensive topographic features within a range of 5 km from a focused point, and are free from such defects as weak to noises of local calculations. Further, the openness is calculated as an average of overground angles or underground angles in eight azimuths, and substantially orientation-independent.

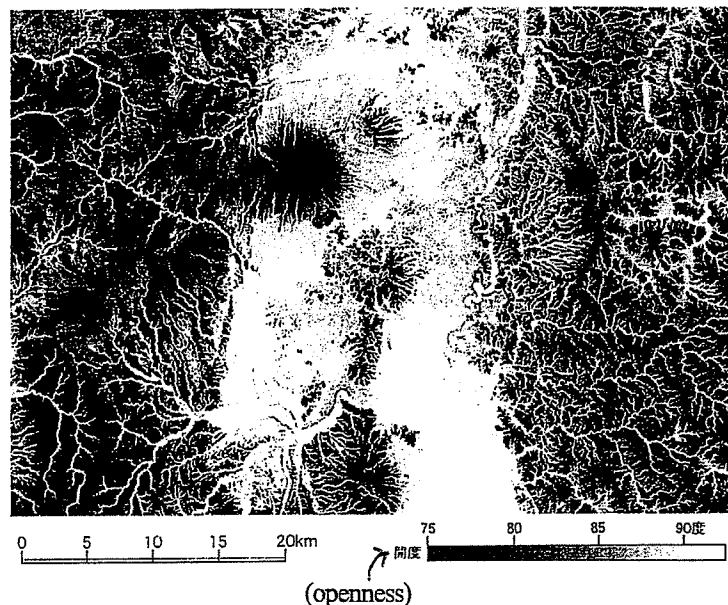


Fig. 7: Underground openness map for $L = 5$ km

4.4 0.5 km overground openness

Fig. 8 is an overground openness map for $L = 0.5$ km. Though being alike with Fig. 6 as an overground openness, Fig. 8 is stronger in black-to-white contrast, with more appearing black and white lines. Since the openness has a non-increasing characteristic with respect to L as described, a topographic feature of a closer region to a focused sample point is to be extracted, as a smaller L is designated. Those ridgelines and valley lines appearing in Fig. 6 will appear in Fig. 8 as well, but all ridgelines and valley lines in Fig. 8 will not appear in Fig. 6. In this sense, macroscopic topographic features are extracted in Fig. 6, and microscopic topographic features are extracted in Fig. 8, instead.

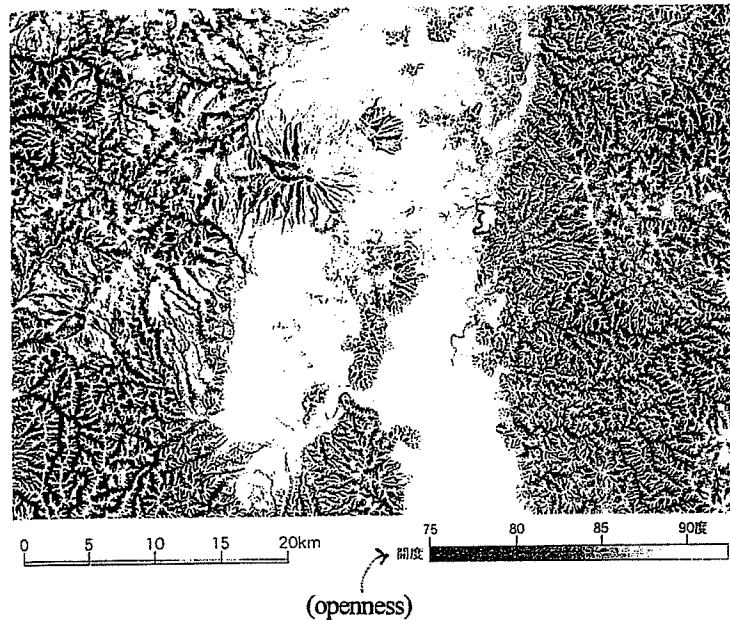


Fig. 8: Overground openness map for $L = 0.5$ km

4.5 0.5 km underground openness

Fig. 9 is an underground openness map for $L = 0.5$ km. In this case also, due to the difference in calculation distance L , relative to Fig. 7., the black-to-white contrast is stronger, with more appearing valley lines. In particular, among others, in foot parts of Mt. Iwate as well as volcanic districts of Akita Komagatake and Hachimantai at the west side of Mt. Iwate, minute valley lines can be seen, which are unobservable in Fig. 7.

5

10

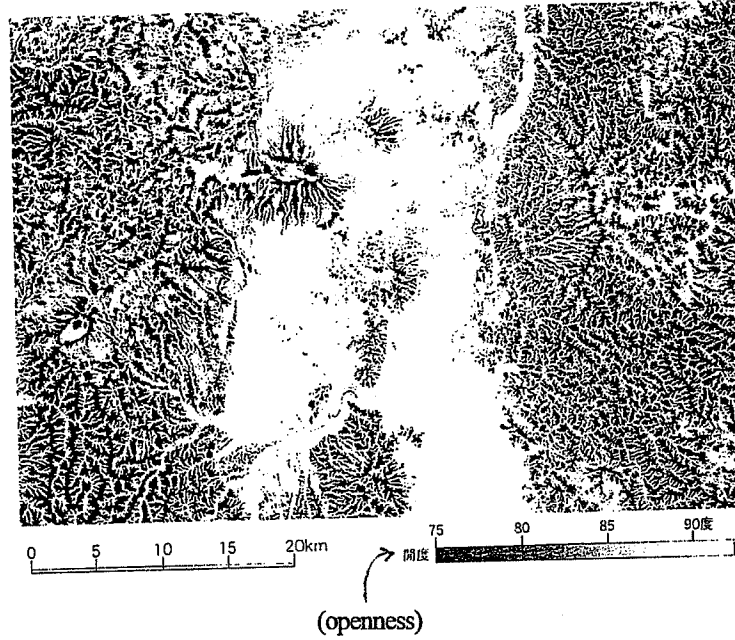


Fig. 9: Underground openness map for $L = 0.5$ km

4.6 Topographic map by Laplacian

15

The UTM-DEM of target area was processed by Laplacian operation, with a result shown in Fig. 10. The Laplacian is a known image processing measure for edge detection based on a spatial secondary differentiation⁸⁾.

20

25

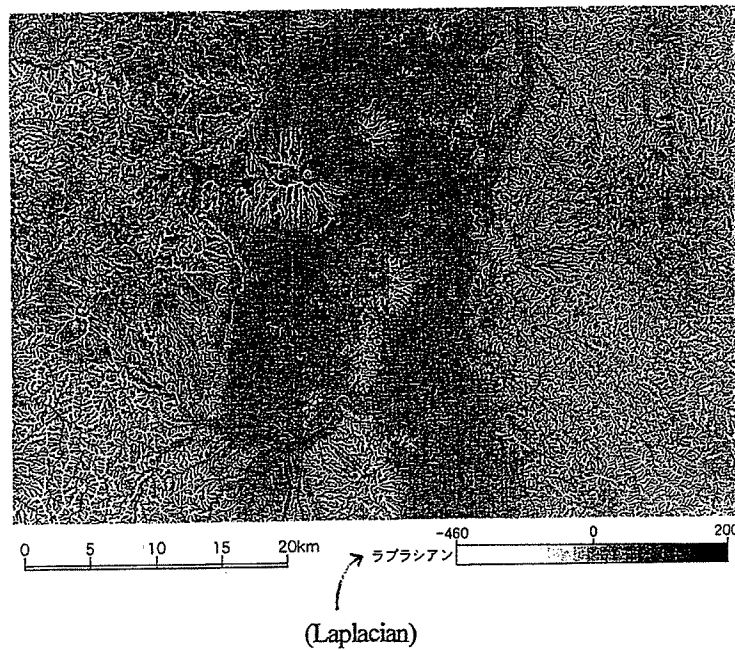


Fig. 10: Result of Laplacian operation processing

30

Generally, the Laplacian provides a large positive value to convex terrain, and a small negative value to concave terrain. Further, it gives near-zero values to landforms with small gradient variations, such as a flatland or monotone slope. In representation in the figure, the larger a Laplacian value is the more black the site becomes, and the smaller it is the more white the site becomes. Though actually appearing as black and white lines, the ridgelines and valley lines are matte, and have poor information readable, in comparison with Figs. 6 to 9.

5. Conclusion

In this paper we have proposed, as new measures for representation of topographic features, an overground openness and an underground openness under a designated distance for calculation using a digital elevation model. Actually, for a peripheral area of Mt. Iwate, we prepared overground openness maps and underground openness maps with different calculation distances. The overground openness maps and underground openness maps adequately reflected features of convex landforms and concave landforms, respectively. It also has turned out that macroscopic topographic features can be extracted by adoption of a large calculation distance, and microscopic topographic features can be extracted by adoption of a small calculation distance. In comparison with conventional relief maps or maps by differential operations for such subjects, the above subject maps contain rich topographic information, with possible expectation to open a new frontier for topographic and geographic decipher. Now, we are preparing overground openness maps and underground openness maps of extended target areas, with confirmed appearance of featuring images in figures, covering terrace, volcano, alluvial fan, hill side, faulting, and other landforms, as well. The opennesses have abilities to be effectively employed for topographic decipher and classification, as well, so we are repeating discussions with experts in associated fields. We want to report results of such researches another time.

References:

- 1) Horn, B.K., *Hill shading and the reflectance map*, *Proc. Of the IEEE*, Vol. 69, No. 1, pp. 14-47, 1981.
- 2) Weibel R. and Heller M., *Digital terrain modeling*, pp. 269-297, Chap. 19, *Geographical Information Systems, Longman Scientific & Technical*, 1991.

- 3) *Peucker, T. K. and Douglas, D. H., Detection of surface specific points by local parallel processing of discrete terrain elevation model, Computer Graphics and Image Processing, Vol. 4, No. 3, pp. 375-387, 1975.*
- 4) *Jenson, S. and Diminique, J., Extracting topographic structure from digital elevation data for geographical information system analysis, Photogrametric Engineering and Remote Sensing, Vol. 54, No. 11, pp.1593-1600, 1988.*
- 5) *Lee, J., Digital analysis of viewshed inclusion and topographic features on digital elevation models, Photogrametric Engineering and Remote Sensing, Vol. 60, No. 4, pp. 451-456, 1994.*
- 10 6) *Blaszczynski, J. S., Landform characterization with geographic information systems, Photogrametric Engineering and Remote Sensing, Vol. 63, No. 2, pp.183-191, 1997.*
- 7) *Shouhichi NOMURA, Map projecting method, (foundation) Japan Map Center.*
- 8) *Rosenfeld, A. and Kak, C., Digital picture processing, second edition, Vol. 1, Academic Press, New York, 1982.*
- 15 9) *Michio NOGAMI, Introduction to minute DEM and watershed topographic measurement, Geography critique, 68A-7, pp.465-474, 1995.*

